Chapter

Steered Beam Adaptive Antenna Arrays

Amin H. Al Ka'bi

Abstract

In this chapter, the performance of steered beam adaptive arrays is presented with its corresponding analytical expressions. Computer simulations are used to illustrate the performance of the array under various operating conditions. In this chapter, we ignore the presence of mutual coupling between the array elements. The principal system elements of the adaptive array consist of an array of sensors (antennas), a pattern-forming network, and an adaptive pattern control unit or adaptive processor that adjusts the variable weights in the pattern-forming network. The adaptive pattern control unit may furthermore be conveniently subdivided into a signal processor unit and an adaptive control algorithm. The manner in which these elements are actually implemented depends on the propagation medium in which the array is to operate, the frequency spectrum of interest, and the user's knowledge of the operational signal environment.

Keywords: antennas, adaptive arrays, steered beam, electromagnetic waves, pointing errors

1. Introduction

Antenna systems can be classified as omnidirectional, directional, phased array, or adaptive array. An omnidirectional antenna (also called isotropic antenna) has equal gain in all directions. On the other hand, directional antennas have more gain in certain directions and less in others. A phased array antenna uses an array of antenna elements and combines the signals received on these elements with appropriate phase shifts to form the output of the array. The direction of the maximum gain (main beam) can be controlled by adjusting the phase between the elements of the array. For the case of narrow-band signals, which is considered here, the term adaptive antenna is used when the weights (magnitudes/gains and phases) of the signals induced on the array elements are regularly updated before combining, in order to control the radiation pattern of the array dynamically according to the requirements of the system [1–3].

In an optimal adaptive antenna array system, the gain and phase of each antenna element are adjusted to achieve the optimal performance of the array in some sense. For example, one basis for adjusting the gain and phase of each element is to obtain maximum output signal-to-interference-plus-noise ratio (*SINR*) by canceling undesired interferences while receiving the desired signal. Such an arrangement is referred to as optimal combining in the mobile communication literature [2, 4].

Desired signal tracking with an adaptive array can be accomplished in various ways. One can either supply a reference signal in the feedback loop of the array and use an adaptive algorithm such as the least mean squares algorithm (LMS); or one can inject steering weights into the feedback loops based on the prior knowledge of the arrival angle of the desired signal and use optimal combining to adjust the weights of the array; or as a third approach, blind adaptation can be used which is similar to LMS but it does not require a reference signal. The second approach is vastly simpler than the first one since no reference signal is required at all. The only difficulty with this approach is that the designer must know the arrival angle of the desired signal accurately [5]. In many situations, however, the angle of arrival of the desired signal is known to some degree of accuracy. The disadvantages of the third approach lie in the fact that the blind adaptation is too slow and/or complex in the mobile environment, because fading and movement may introduce sudden large variations in levels of desired signals and interferers, which complicate the blind adaptation process.

This chapter focuses on the second approach, and in particular optimal combining steered beam adaptive arrays. Such arrays typically aim to maximize the *SINR*. The achieved *SINR* depends largely on the "pointing error" in steering the main beam of the array toward the direction of the desired signal [5–7]. Therefore, the effect of pointing error will be discussed extensively, and it will be considered as one of the assessment criteria of the array performance.

Here are some basic concepts and considerations related to beam formation using antenna arrays mounted on base stations:

a. Formation of multiple beams: The antenna array is used to form multiple static beams to cover the whole cell site. This is the simplest configuration but leads to waste in transmitted power.

b. Formation of adaptive beams: The array is used to find the location of each mobile, and beams are formed to cover different mobiles or groups of mobiles by tracking their locations adaptively.

c. Formation of nulls: In general, an N-element antenna array has $N - 1$ degrees of freedom; that is, it can null out $N - 1$ interference signals. By forming nulls in the antenna pattern toward interfering mobiles, the co-channel interference can be reduced in two ways. In the transmit mode, less energy is transmitted from the base toward these mobiles, reducing the interference from the base to them. In the receiving mode, formation of nulls reduces the contribution from these mobiles at the base. Consequently, *SINR* can be improved and thus, the capacity of the communication system can be increased. Moreover, nulling of interferers can allow for low-power transmitters to coexist with high-power transmitters without a substantial decrease in performance [8]. If the number of interferers exceeds the number of array elements, the array tends to form a radiation pattern such that the output *SINR* is maximized. In this case, the interference signals are not perfectly nulled, and the performance of the array is significantly affected, as will be discussed in Section 2 [9–12].

It is assumed that the elements of the adaptive array are short dipoles (such that their individual radiation patterns are very close to isotropic antennas) and arranged in vertical positions with their beams that are formed in a broadside direction. The array elements are spatially arranged in such a way to provide sufficient coverage over the expected range of directions of the desired signal. The

type and the arrangement of the elements set significant limitations on the maximum capability of the array system, in terms of its capability to detect the desired signal and to null the interference signals with acceptable *SINR* [13, 14].

The individual output of each antenna element is fed to the pattern-forming network shown in **Figure 1**, where outputs are weighted by complex weights (amplifiers/attenuators and phase shifters), and then added to generate the overall output of the array. The values of the weights (which are determined by the adaptive signal processor based on the available information and the physical arrangement of the individual isotropic sensor elements) determine the overall array beam sensitivity pattern.

The steered beam adaptive arrays are based on the concept of maximizing the desired-to-undesired (interference plus thermal white noise) signal ratio at the output of the array [1–3, 5, 9]. Conceivably, this leads to placing nulls in the directions of the interference and noise while placing a maximum gain in the direction of the desired signal.

2. Signal model

The steered beam adaptive arrays are based on the concept of maximizing the desired-to-undesired (interference plus thermal white noise) signal ratio at the output of the array [2, 3]. Conceivably, this leads to placing nulls in the directions of the interference and noise while placing a maximum gain in the direction of the desired signal.

Consider the N-element adaptive array shown in **Figure 1**, receiving complex analytic signals[1] where the ith complex analytic signal is denoted by $\overline{x}_i(t)$ and the ith complex weight is denoted by w_i . We define the signal vector,

$$X = [\overline{x}_1(t), \overline{x}_2(t), \overline{x}_3(t), \ldots, \overline{x}_N(t)] \tag{1}$$

This signal vector can be split into a desired signal term, an interference term, and a thermal noise term,

$$X = X_d + X_I + X_n \tag{2}$$

The output signal of the array may be split in a similar way,

$$\overline{S}_o(t) = X^T w = \overline{S}_d(t) + \overline{S}_I(t), + \overline{S}_n(t) \tag{3}$$

The desired signal power, interference power, and noise power at the output of the array are then given as

$$P_d = E\{\left|\overline{S}_d(t)\right|^2\} \tag{4}$$

$$P_I = E\{\left|\overline{S}_I(t)\right|^2\} \tag{5}$$

$$P_n = E\{\left|\overline{S}_n(t)\right|^2\} \tag{6}$$

where $E\{.\}$ denotes expectation with respect to time. The steering vector adaptive array is based on the concept of maximizing the ratio of the desired signal

[1] Complex analytic signals correspond to real passband signals, as a result of complex baseband signal processing.

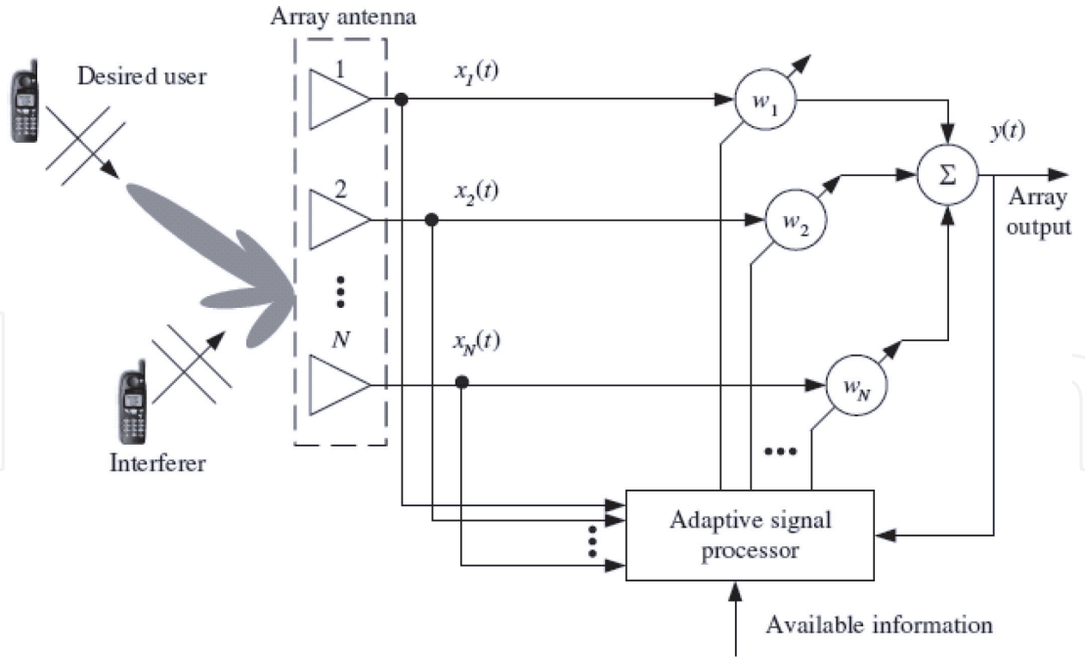

Figure 1.
Block diagram of an adaptive antenna array system.

power P_d to the undesired signals powers $P_u = P_I + P_n$; that is, to adjust the weights so that the quantity

$$SINR = \frac{P_d}{P_u} = \frac{P_d}{P_I + P_n} \tag{7}$$

is maximized. In his paper [3], Applebaum proved that the feedback loop shown in **Figure 2** maximizes the output *SINR* of the array. More details on this are given in the next section.

In **Figure 2**, it should be noted that the *N*-element array has *N* feedback loops, where w_{0j} is the *j*th component of the steering vector $\overline{w}_0$, and *k* is the feedback loop gain. In the absence of any incoming signals, the weight vector *w* is a scalar complex-valued multiple of $\overline{w}_0$. In this case, the array has a pattern determined by $\overline{w}_0$, and this pattern is called the quiescent pattern of the array [2, 3]. $\overline{w}_0$ can be chosen to obtain a desired pattern from the array (i.e., it can be determined by the user's knowledge of the arrival angle of the desired signal). Because the vector $\overline{w}_0$ steers the main beam of the quiescent antenna pattern, it is usually called the steering vector. This steering vector is vulnerable to errors. One kind of error is the pointing error, which is studied extensively in this research in order to mitigate its effect on the performance of the adaptive array.

3. Problem formulation

Figure 3 shows a linear *N*-isotropic element adaptive array with inter-element separation distances $y_1, y_2, y_3, \ldots, y_{N-1}$, which, in general, may be nonuniform. Here, we consider the case of one desired signal and *M* interference signals, lying in the same 2-D plane containing the linear array.

The received signal from the *i*th element (which is assumed to be a complex random process) is multiplied by a complex weight w_i and summed with the other $N - 1$ output signals to produce the array output $\overline{S}_o(t)$. Using the feedback loop

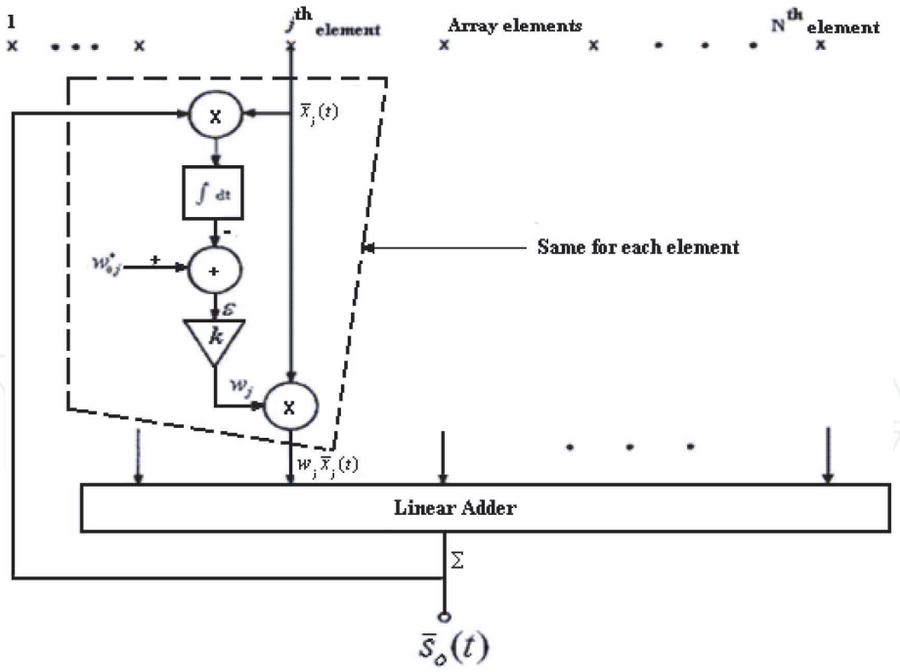

Figure 2.
Feedback loop of the steering vector adaptive array [3].

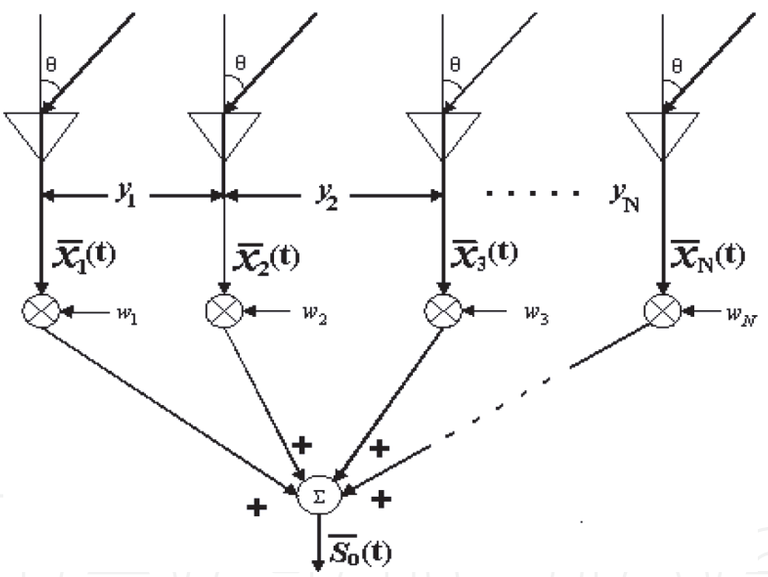

Figure 3.
N-*elements adaptive array with nonuniform spacings.*

configuration of **Figure 2**, the steady-state weight vector that maximizes the output *SINR* is given by [2, 3]:

$$w = [w_1, w_2, w_3, \ldots, w_N]^T = [I + k\Phi]^T \overline{w}_0 \tag{8}$$

where, $\Phi = E\{X^* X^T\}$ is the covariance matrix of the received signal, and $\overline{w}_0 = [w_{10}, w_{20}, w_3, \ldots, w_{N0}]^T$ is the steering vector of the array [1], I is the identity matrix, k is the feedback loop gain, T denotes transpose, * denotes complex conjugate, E {.} denotes the expectation, and X is the received signal vector as defined in Eq. (1). The received signal of the jth element is given by the following:

$$\overline{x}_j(t) = \overline{S}_{dj}(t) + \sum_{i=1}^{M} \overline{S}_{Iij}(t) + \overline{S}_{nj}(t), \mathrm{j} = 1, 2, \ldots, \mathrm{N} \tag{9}$$

where $\overline{S}_{dj}(t)$ is the signal induced on the jth element due to the desired signal, $\overline{S}_{Ij}(t)$ is the signal induced on the jth element due to the ith interference signal, M is the number of interference signals, and $\overline{S}_{nj}(t)$ is the white thermal noise at the jth element, which has zero mean and is uncorrelated with other thermal noise signals such that

$$E\left[\overline{S}_{ni}(t)\overline{S}_{nj}(t)\right] = \sigma^2\delta_{ij} \tag{10}$$

where σ^2 is the variance of the thermal white noise, and δ_{ij} is the Kronecker delta function. In this array, uniform plane waves are assumed to be incident on the sensors of the array, and the medium is assumed to be linear and its only effect on the signals is a time delay. Hence, the desired signals $\overline{S}_{d1}(t), \overline{S}_{d2}(t), \ldots, \overline{S}_{dN}(t)$ differ by an inter-element propagation time

$$T_{dp} = \left(\frac{y_p}{c}\right)\sin\theta_d \tag{11}$$

where c denotes the velocity of light, θ_d is the arrival angle of the desired signal, y_p is the inter-element spacing between the pth element and the $(p+1)$th element, and T_{dp} denotes the propagation time between the pth element and the $(p+1)$th element. Hence

$$\overline{S}_{dj}(t) = \overline{S}_{d1}\left(t - \sum_{p=1}^{j-1} T_{dp}\right).\gamma_d, \mathrm{j} = 1, 2, \ldots, \mathrm{N} \tag{12}$$

where $\gamma_d = \exp\left(-j\omega_c\sum_{p=1}^{j-1}T_{dp}\right)$, and ω_c is the center frequency of the power spectral density of the desired signal. Similarly, $\overline{S}_{Ij}(t)$ is given by the following:

$$\overline{S}_{Iij}(t) = \overline{S}_{Ii1}\left(t - \sum_{p=1}^{j-1} T_{Iip}\right).\gamma_I, \mathrm{j} = 1, 2, \ldots, \mathrm{N} \tag{13}$$

where $\gamma_I = \exp\left(-j\omega_c\sum_{p=1}^{j-1}T_{Iip}\right)$, i denotes the ith interference signal, j denotes the jth sensor element of the array, and

$$T_{Ipi} = \left(\frac{y_p}{c}\right)\sin\theta_{Ii} \tag{14}$$

where θ_{Ii} is the arrival angle of the ith interference signal. The desired and the interference signals are assumed to have zero mean, and are stationary and statistically independent from each other and the thermal noise. This applies in many cases, especially in narrowband-faded signals, with different Directions of Arrival (DOA's).

Using these results in Eq. (8), together with the initial steering vector $\overline{w}_0$, a signal component-based expression for the steady-state weight vector of the array can be determined.

With the aim of obtaining a complete signal component-based expression for the steady-state weight vector w of Eq. (8), we now focus on the steering vector $\overline{w}_0$. The steering vector $\overline{w}_0$ is chosen to provide a beam maximum of the quiescent pattern in a given direction θ_{max}. It can be noted that a CW signal from an angle θ_{max} will produce a signal vector:

$$X = \left[1, e^{-j\beta l_1 \sin\theta_{max}}, e^{-j\beta(l_1+l_1)\sin\theta_{max}}, \ldots, e^{-j\beta\sum_{i=1}^{N-1} l_i \sin\theta_{max}}\right].e^{j\omega_c t} \tag{15}$$

where ω_c is the center frequency of the power spectral density of the desired signal and $\beta = \frac{2\pi}{\lambda}$ is the wave number of the desired signal. The output of the array for such a signal would be

$$\overline{S}_o(t) = X^T w \tag{16}$$

so that

$$\overline{S}_o(t) = \left[w_1, w_2 e^{-j\mu_1} + w_3 e^{-j\mu_2} + \ldots + w_N e^{-j\mu_{N-1}}\right].e^{j\omega_c t} \tag{17}$$

where $\mu_i = \left(\sum_{j=1}^{i} l_j\right)\beta \sin(\theta_{max})$.

The quiescent pattern of the array will have a maximum on this signal if

$$w_1 = w_2 e^{-j\mu_1} = w_3 e^{-j\mu_2} = \ldots = w_N e^{-j\mu_{N-1}} \tag{18}$$

Therefore, for a given θ_{max} and according to the phased array theory, $\overline{w}_0$ should be chosen as

$$\overline{w}_0 = \left[e^{-j\mu_{N-1}}, \ldots, e^{-j\mu_2}, e^{-j\mu_1}, 1\right]^T \tag{19}$$

Using this $\overline{w}_0$, the steady-state weight vector w may then be calculated from Eq. (8), that is, $w = [I + k\Phi]^T \overline{w}_0$. Here, it should be noted that the difference between θ_{max} and the actual direction of the desired signal θ_d is called the pointing error (θ_{per}) of the main beam of the array.

The signals $\overline{S}_d(t)$ and $\overline{S}_{I1}(t)$, $\overline{S}_{I2}(t)$, $\overline{S}_{I3}(t)$, ..., $\overline{S}_{IN-1}(t)$ are defined such that the normalized autocorrelations in Eqs. (20) and (21) could be found; thus, they are each assumed to be a wide sense stationary random process with flat band-limited power spectral density centered at ω_c.

Using Eq. (7), the steady-state weight vector w may then be calculated from Eq. (1). The output power of the desired signal can be written as

$$P_d = S_d\left[\sum_{n=1}^{N}\left|w_N\right|^2 + \sum_{i=1}^{N-1}\sum_{m=2}^{N} 2\,Re\left\{w_N w_m^* \rho_{d_{ij}}\right\}\right], for\ m > n \tag{20}$$

where $\rho_{d_{ij}}$ is the normalized autocorrelation between the desired signals coming from the ith and jth antenna elements. The output power of the i^{th} interference signal is [5]:

$$P_{I_i} = S_{I_i}\left[\sum_{n=1}^{N}\left|w_N\right|^2 + \sum_{i=1}^{N-1}\sum_{m=2}^{N} 2\,Re\left\{w_N w_m^* \rho_{I_{ipj}}\right\}\right], for\ m > n \tag{21}$$

and the output power of the thermal noise is given by the following:

$$P_n = \sigma^2 \sum_{n=1}^{N}\left|w_N\right|^2 \tag{22}$$

From P_d, $\sum_{i=1}^{M} P_{I_i}$, and P_n, the output *SINR* can be computed as

$$SINR = 10 * \log\left(P_d / \left(\left(\sum_{i=1}^{M} P_{I_i}\right) + P_n\right)\right) \tag{23}$$

which can be used as a measure of the performance of the adaptive array in the sequel. The radiation/sensitivity pattern of the array can be calculated from

$$E(\theta) = 20 \log\left(w_1 + w_2 e^{-j\mu_1} + w_3 e^{-j\mu_2} + \ldots + w_N e^{-j\mu_{N-1}}\right) \tag{24}$$

where $\mu_i = \left(\sum_{j=1}^{i} y_j\right)\beta sin\theta$. Now, all of the equations needed to compute the output SINR as a function of the input signal-to-noise ratio (SNR), input interference-to-noise ratios, arrival angles of the desired and interference signals, and bandwidths of the desired and interference signals are readily available. MATLAB application is used to simulate the operation of the array.

4. Performance of the array

In this section, the performance of steered beam adaptive array with uniform inter-element spacing of ($\lambda/2$) will be studied with respect to various operating conditions,[2] including pointing error, feedback loop gain, input *SNR*/element, input *INR*/element, and DOAs and bandwidths of the desired and interference signals.

Consider first the case where there is no interference. **Figure 4** shows the output SINR of a three-element array as a function of pointing error (θ_{perr}), which is the difference between the DOA of the desired signal (θ_d) and the direction of the main beam of the array (θ_{max}). Several curves are shown for different input *SNR*'s/element. The curves are computed for feedback loop gain K = 0.1, and zero desired signal bandwidth (B_d = 0).

From **Figure 5**, it can be seen that the sensitivity of the array to pointing errors increases with increasing *SNR*. For example, if *SNR* = 5 dB, the array provides output *SINR* > 5B if the pointing error margin lies within $\pm 15^o$, but for *SNR* = 40 dB,

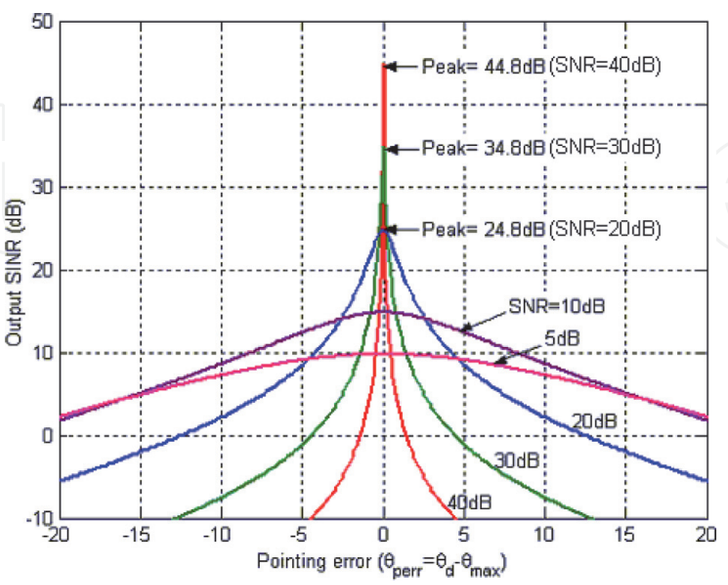

Figure 4.
Output SINR vs. θ_{perr}. Three-element array, $\theta_d = o^o$, K = 0.1, and B_d = 0. No interference.

[2] The nonuniformly spaced adaptive arrays will be studied in the next chapters.

the array output exceeds 5 dB only if the pointing error lies within $\pm 0.8^o$. The explanation of this behavior is illustrated in **Figure 5**, where typical radiation patterns are plotted using Eq. (24), under the same conditions as in **Figure 4**.

In **Figure 5(a)**, the pointing error $\theta_{perr} = \theta_d - \theta_{max}) = 0^o$, and in **Figure 5(b)**, $\theta_{perr} = 5^o$. For $\theta_{perr} = 0^o$, it can be seen that as the *SNR* increases, the overall radiation pattern magnitude is reduced. As the pattern amplitude drops, both the desired signal power and the thermal noise power drop in proportion. Hence, the output *SINR* remains relatively unaffected by this change in pattern amplitude. For $\theta_{perr} = 5^o$, the pattern behavior is quite different. Here, it can be seen that as the *SNR* increases, the array increasingly suppresses the desired signal. Since it can do this without lowering the overall pattern amplitude, the result is to reduce the desired signal power without reducing the thermal noise power. This accounts for the behavior seen in **Figure 4**. However, in most system designs, achieving maximum gain is not the most important objective. What matters most is achieving *SINR* at the output of the array that exceeds a certain threshold.

The effect of increasing the number of array elements is depicted in **Figure 6**. When comparing the curves in this figure with those in **Figure 4**, it can be seen that the five-element array is more sensitive to pointing errors than the three-element

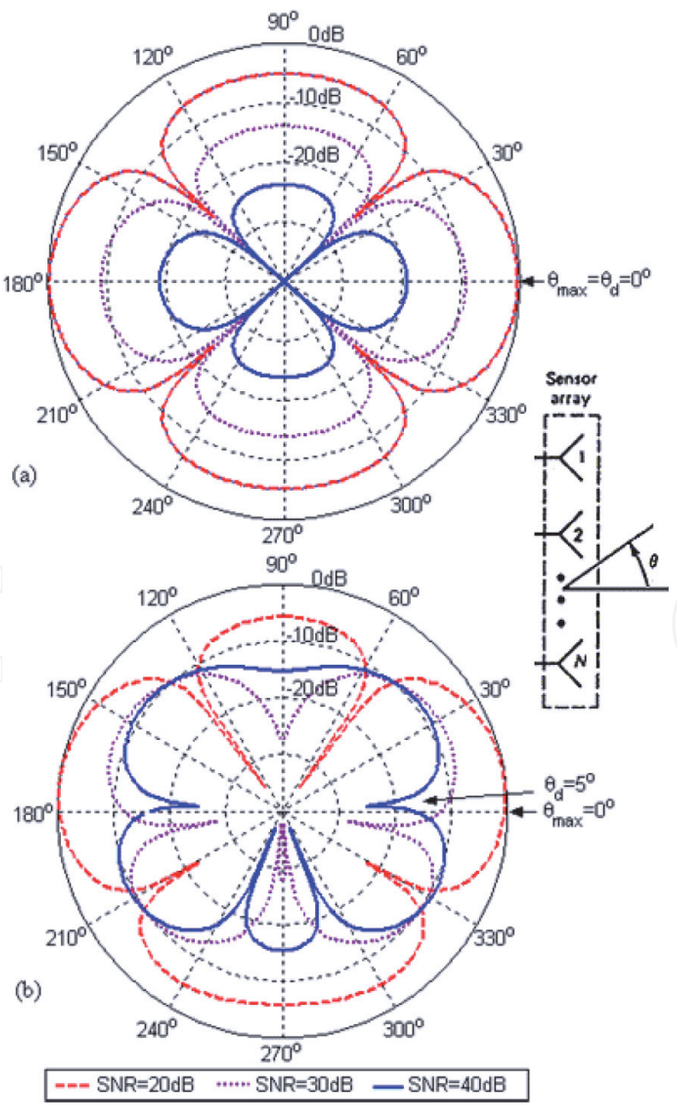

Figure 5.
Radiation patterns of three-element array. K = 0.1, with different SNR's. No interference. (a) Pointing error $(\theta_{perr} = \theta_d - \theta_{max}) = o^o$. *(b) Pointing error (error* $(\theta_{perr} = \theta_d - \theta_{max}) = 5^o$.

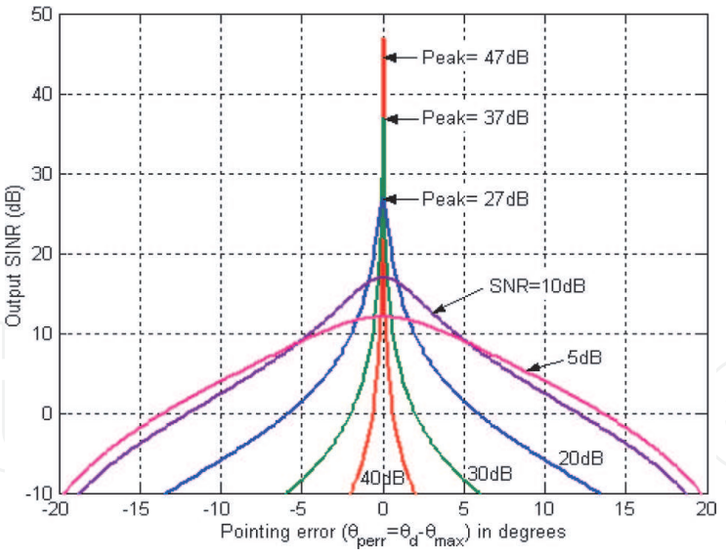

Figure 6.
Output SINR *vs. pointing error. Five-element array,* $\theta_d = 0^o$, $K = 0.1$. *No interference.*

array. For example, when *SNR* = 5 dB, the array provides output *SINR* > 5 dB, as long as $-9^o \leq \theta_{perr} \leq 9^o$.

The explanation of this behavior lies in the fact that the directivity of the array increases by increasing the number of its elements, as illustrated in **Figure 7**. Here, the 3-dB beamwidth of the main beam for the five-element array is less than that of the three-element array.

A different perspective on these results may be gained by plotting the output *SINR* as a function of input *SNR*. **Figure 8** shows several curves for the three-element array with different values of pointing error (θ_{perr}). This figure shows that the beam-pointing error that can be tolerated is essentially a matter of dynamic range. For example, if $\theta_{perr} = 5^o$, the output *SINR* is greater than 5 dB only for

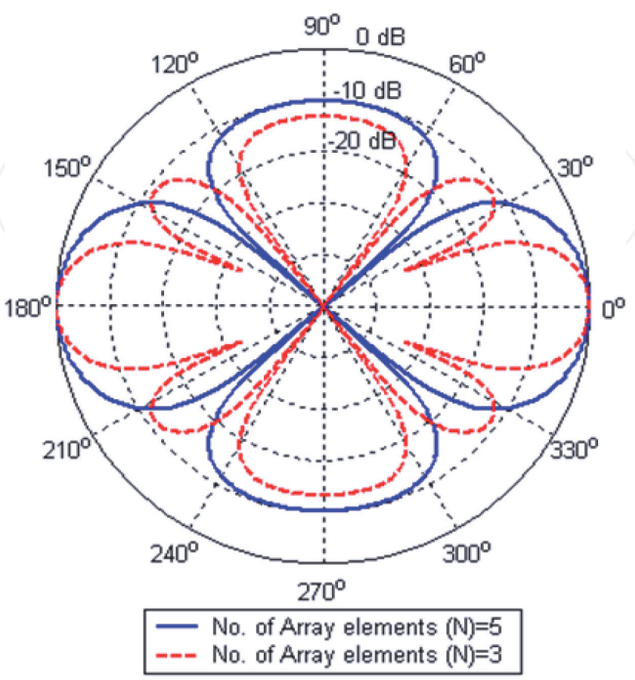

Figure 7.
Normalized radiation patterns of three- and five-element arrays. $\theta_d = 0^o$, *pointing error* $(\theta_{perr} = \theta_d - \theta_{max}) = 0^o$ $(K = 0.1)$. *No interference.*

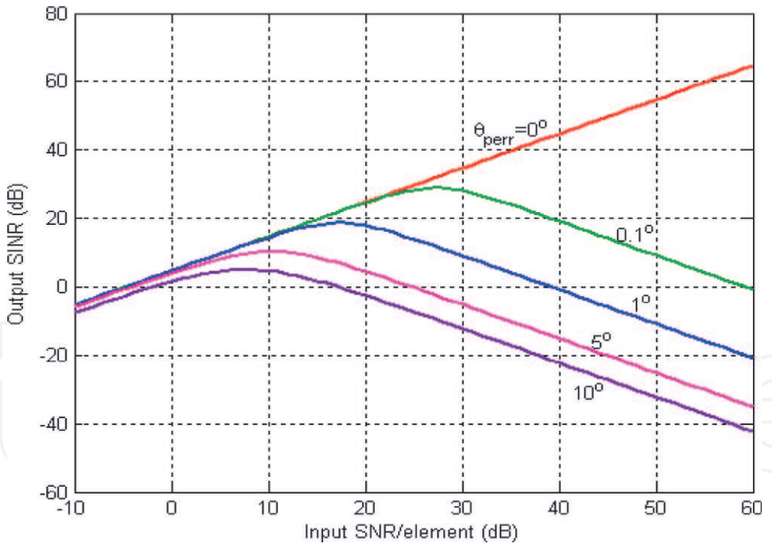

Figure 8.
Output SINR vs. input SNR/element. Three-element array. $\theta_d = 0^o$, K = 0.1, with different values of pointing error ($\theta_{perr} = \theta_d - \theta_{max}$). No interference.

1 dB $\leq SNR \leq$ 19 dB, whereas if $\theta_{perr} = 0.1^o$, the output $SINR >$ 5 dB for 0 dB $\leq SNR \leq$ 56 dB. Therefore, the greater the desired signal dynamic range we wish to accommodate, the less pointing error (θ_{perr}) we should have.

Until now, we assumed that the feedback loop gains of the array K = 0.1. However, the effect of K on the performance of the array is illustrated in **Figure 9**.

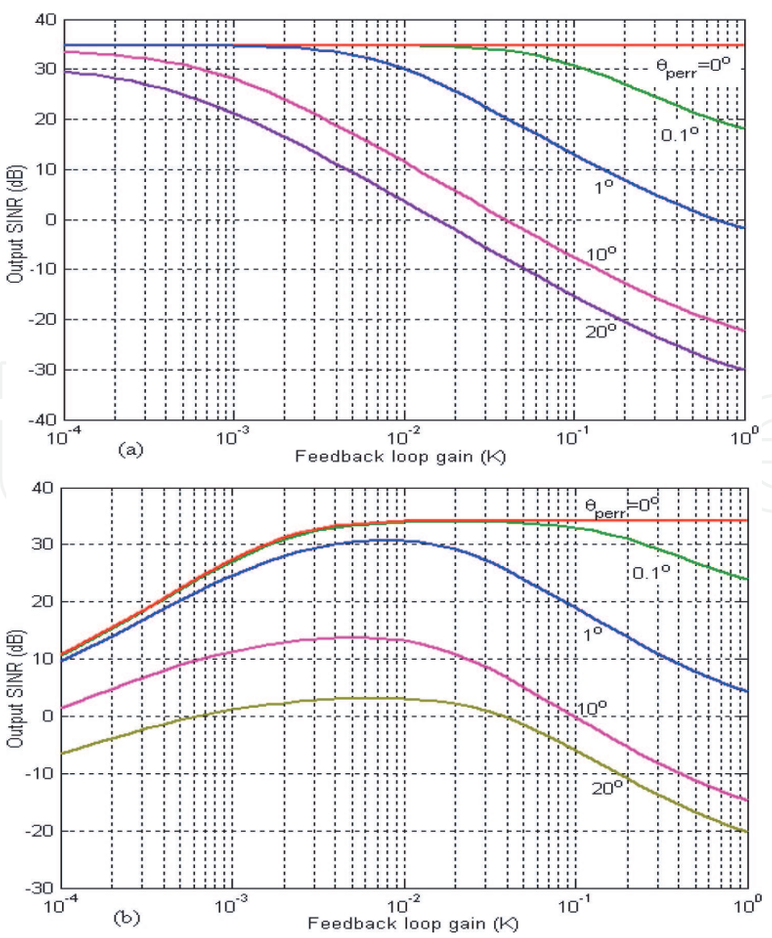

Figure 9.
Output SINR vs. feedback loop gain (K). Three-element array, $\theta_d = 0^o$, and SNR = 30 dB, with different values of pointing error ($\theta_{perr} = \theta_d - \theta_{max}$). (a) No interference. (b) One 40-dB INR interference signal @30°.

In **Figure 9(a)** where interference does not exist, the output *SINR* deteriorates rapidly by increasing *K* because the array tends to suppress the desired signal more, which results in more sensitivity to pointing errors.

On the other hand, when interference exists, **Figure 9(b)** shows that low values of *K*, as well as high values of K, have a negative effect on the performance. This is due to the capability of the array to effectively decrease null interference signals by decreasing *K*. From **Figure 9**, it can be concluded that the most appropriate value for the feedback loop gain is $00.1 \leq K \leq 0.1$. In this chapter, we used $K = 0.1$ as a representative value.

In **Figure 4**, we presented the performance of the array in the absence of interference signals. Now consider the case when interference is present. The equivalent results of **Figure 4** are presented in **Figure 10**, where one interference signal is incident at $\theta_I = 10^o$ with *INR* = 30 dB and zero bandwidth $B_I = 0$.

These curves differ from those in **Figure 4** in several respects. First, for *SNR* < 10 dB, θ_{perr} has less effect on the *SINR* (except for $\theta_{perr} = \theta_I$) than it did with no interference. Second, for higher *SNR*s, the *SINR* again becomes sensitive to θ_{perr}, but much less than that without interference. For example, in **Figure 10** with *SNR* = 30 dB, *SINR* > 5 dB for $-8.25^o \leq \theta_{perr} \leq 3.75^o$, whereas in **Figure 4**, *SNR* = 30 dB yields *SINR* > 5 dB only for $-2.55^o \leq \theta_{perr} \leq 2.55^o$. The reason for this difference is that, in general, with the presence of interference, the array uses its degrees of freedom to form nulls toward the interference. Therefore, the array cannot null the desired signal, as it could without interference.

For further illustration of the performance of the array, **Figure 11** shows the output *SINR* for different DOAs of the desired signal. In this figure, it can be seen that the *SINR* decreases as the DOA of the desired signal gets closer to the DOA of the interference signal. This is because, as expected, the desired signal is increasingly suppressed by the null formed toward the interference signal.

The corresponding results for different DOAs of the interference signal can be seen in **Figure 12**. Again, the *SINR* drops as the interference DOA gets closer to the DOA of the desired signal. **Figure 13** provides extra explanation for these results: the depth of the null toward the interference signal decreases as the DOA of the interference signal gets closer to the DOA of the desired signal. Therefore, more interference power appears at the output of the array.

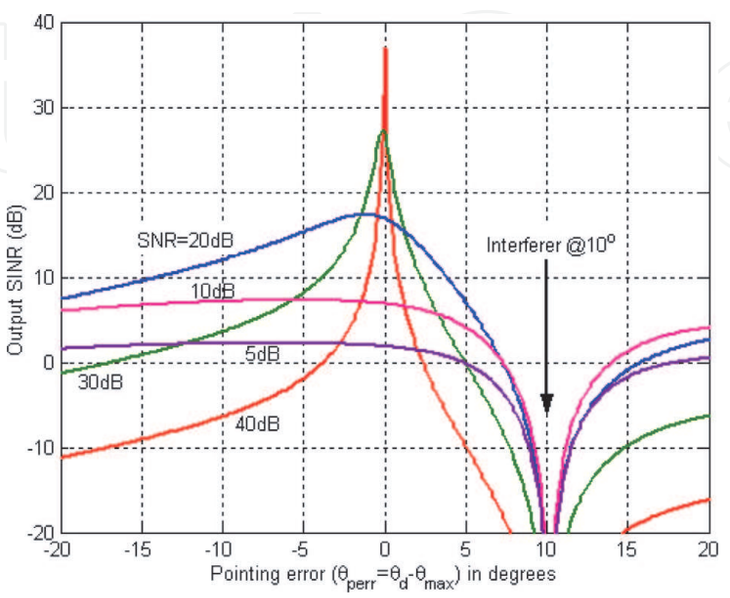

Figure 10.
Output SINR vs. pointing error. Three-element array, $\theta_d = 0^o$, K = 0.1. One 30-dB INR interference signal @ $\theta_I = 10^o$, $B_I = 0$.

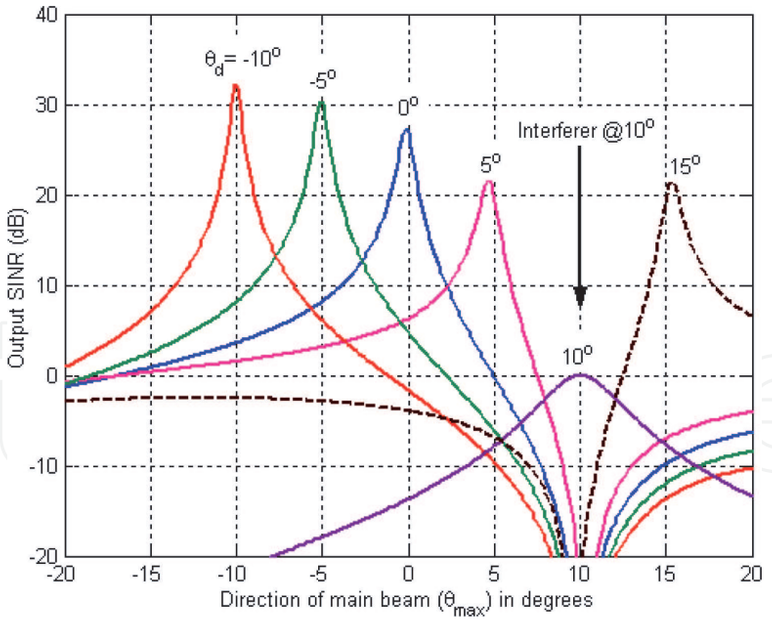

Figure 11.
Output SINR vs. direction of the main beam (θ_{max}). Three-element array, K = 0.1. One 30-dB INR interference signal at $\theta_I = 10^o$. SNR = 30 dB with DOAs of $\theta_d = -10^o, -5^o, -0^o, 5^o, 10^o, 15^o$. $B_d = 0, B_I = 0$.

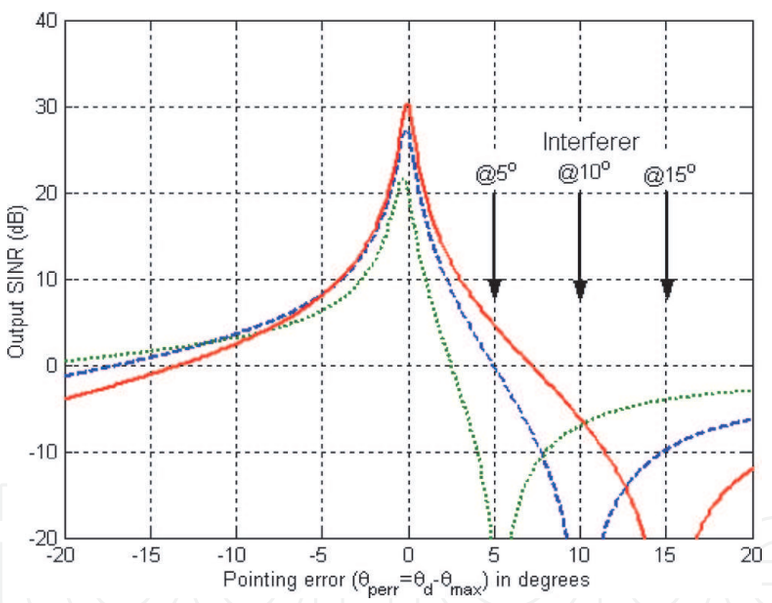

Figure 12.
Output SINR vs. pointing error (θ_{max}). Three-element array, $\theta_d = 0^o$, K = 0.1, $B_d = 0, B_I = 0$. One 30-dB INR *interference signal with DOA @$\theta_I = 5^o, 10^o, 15^o$.*

Figure 14 depicts the output *SINR* vs. the DOA of the interference signal for different values of *INR*, and **Figure 15** depicts the output *SINR* vs. the *INR* of the interference signal with different DOAs. Here, the pointing error $\theta_{perr} = 0^o$.

From these two figures, it can be seen that for the case of $\theta_{perr} = 0^o$, the output *SINR* decreases as the interference signal gets closer to the desired signal (**Figure 14**) and as its *INR* increases (**Figure 15**). It can be noticed that the interference signal is more effectively nulled when its DOA is far away from the DOA of the desired signal. When $\theta_{perr} \neq 0^o$, we get the similar curves as in **Figures 14** and **15** (not shown here), but with lower output *SINR*. The reason is that the complex weights for forming a radiation pattern are selected for the center frequency.

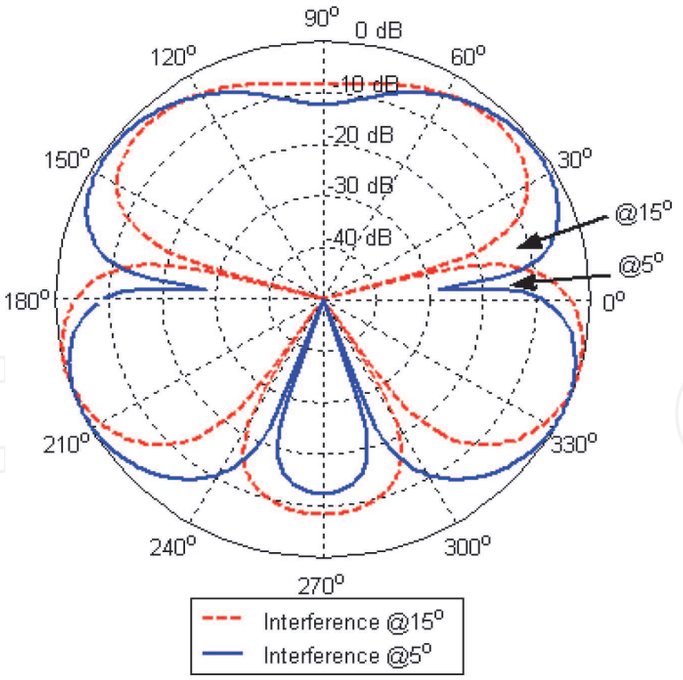

Figure 13.
Normalized radiation patterns for three-element array. $\theta_d = 0^o$*, pointing error* $(\theta_{perr} = \theta_d - \theta_{max}) = 0^o$*,* $B_d = 0, B_I = 0$*. One 30-dB* INR *interference signal with DOA at* $\theta_I = 5^o, 15^o$*.*

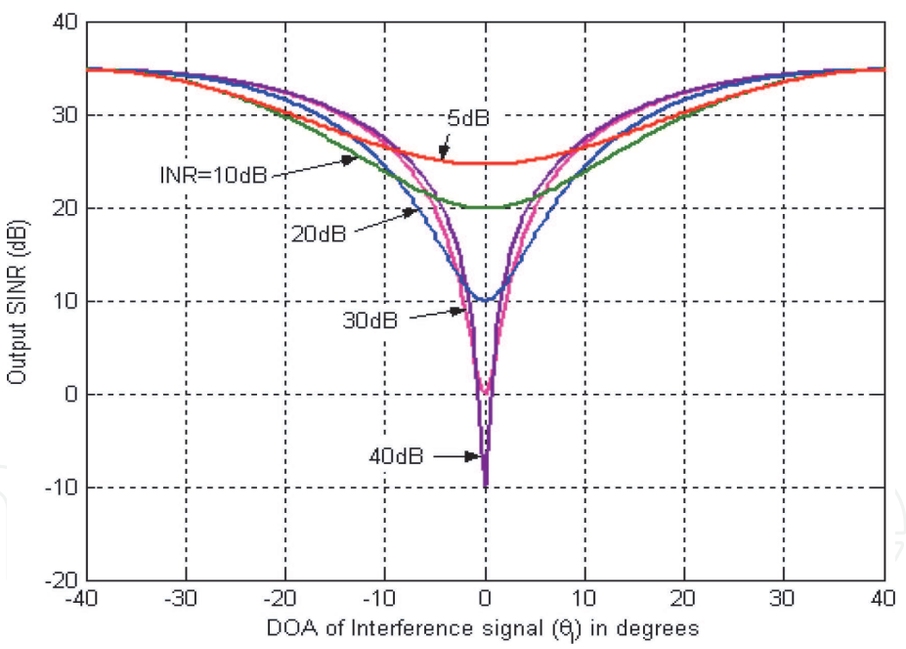

Figure 14.
Output SINR *vs. DOA of the interference signal. Three-element array,* $\theta_d = \theta_{max} = 0^o$*, SNR = 30 dB, K = 0.1, and* $B_d = 0, B_I = 0$*.*

Figure 16 shows the output *SINR* versus the input *SNR* for several values of pointing error θ_{perr}, taking into consideration the effect of the interference signal bandwidth (B_I). Here, it can be seen that the output *SINR* decreases by increasing the interference bandwidth (B_I), due to the decreased efficiency in the null formation toward the interference.

By comparing **Figure 16** with **Figure 8** (where the interference is absent), it can be seen that the performance of the array has been enhanced in the interference case in terms of the dynamic range of the desired signal that can be accommodated

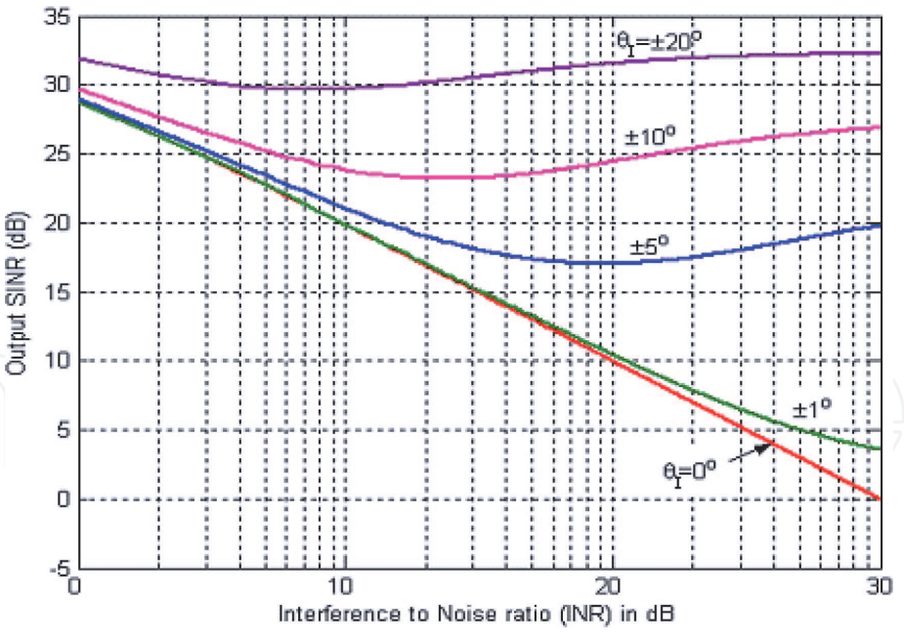

Figure 15.
Output SINR *vs. interference-to-noise ratio (*INR*). Three-element array, $\theta_d = \theta_{max} = 0^o$. SNR = 30 dB, K = 0.1, and $B_d = 0, B_I = 0$, with different DOAs of the interference signal (θ_I).*

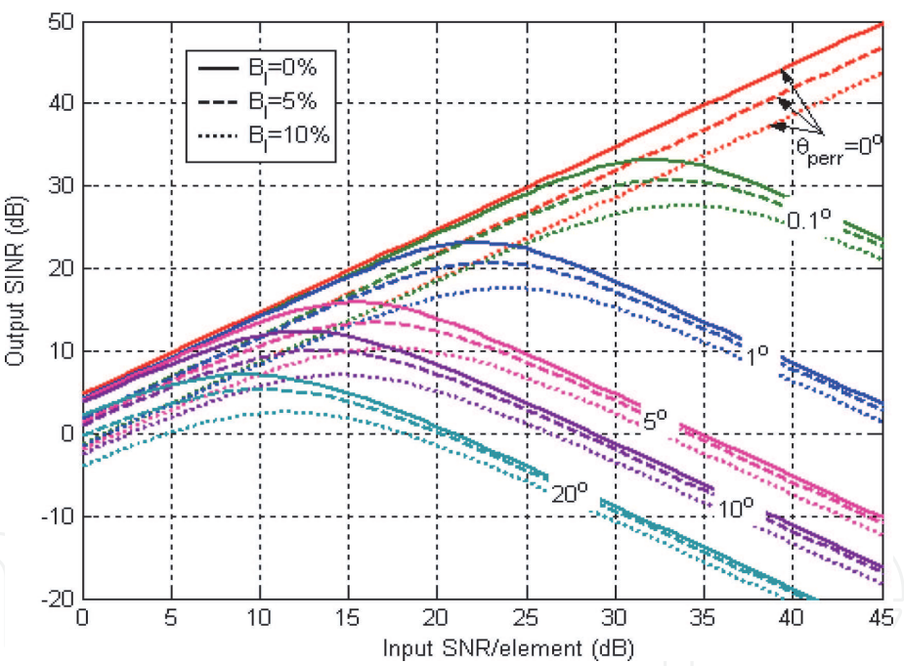

Figure 16.
Output SINR vs. input SNR/element. Three-element array, K = 0.1, and $B_d = 0$, with different values of pointing error ($\theta_{perr} = \theta_d - \theta_{max}$). One 30-dB INR interference signal with DOA@ 30° with different bandwidths (B_I).

for a given θ_{perr}. For example, for $\theta_{perr} = 1^o$ and $B_I = 0$, the interference-free case provides output SINR greater than 5 dB only for 1 dB $\leq SNR \leq$ 34.2 dB, whereas in the presence of interference, the output $SINR >$ 5 dB for 1 dB $\leq SNR \leq$ 43.5 dB.

The interference bandwidth B_I decreases with a decreasing *INR*. This can be concluded from the comparison between **Figures 16** and **17**, where the effect of B_I is insignificant in the latter case.

The effect of the interference signal bandwidth and its *INR* is further explained in **Figure 18**. Here, it can be seen that the effect of the bandwidth of the interference signal is more significant when its *INR* is higher.

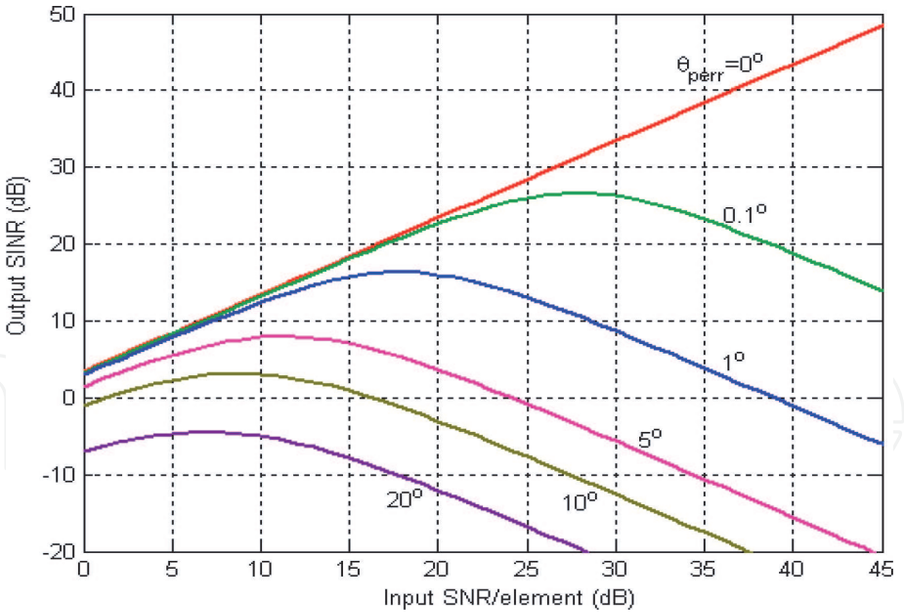

Figure 17.
Output SINR vs. input SNR/element. Three-element array, K = 0.1, and $B_d = 0$, with different values of pointing error ($\theta_{perr} = \theta_d - \theta_{max}$). One 5-dB INR *interference signal with DOA@ 30° and bandwidths ($0\% \leq B_I \leq 20\%$).*

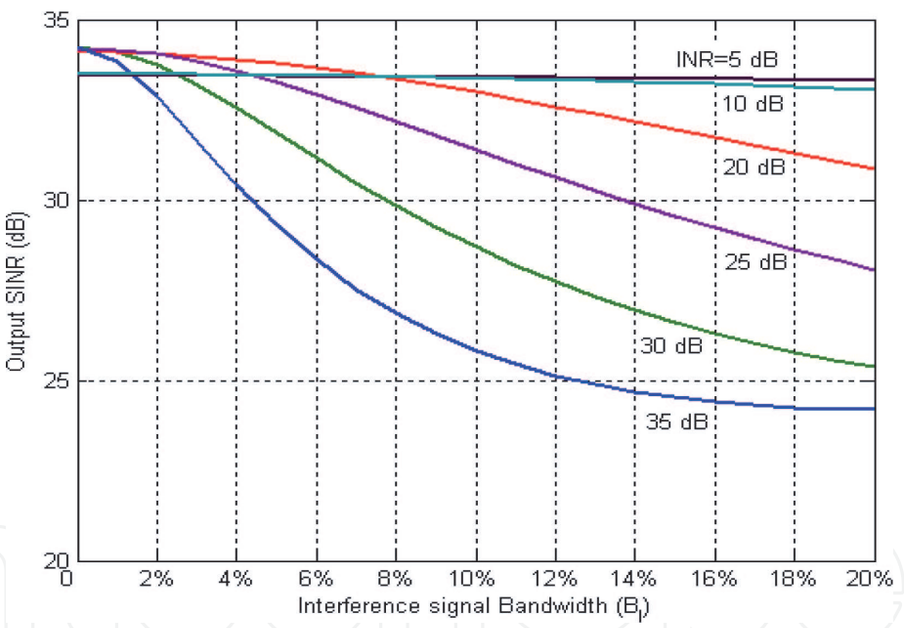

Figure 18.
Output SINR vs. interference signal bandwidth (B_I). Three-element array, K = 0.1, and $B_d = 0$, pointing error ($\theta_{perr} = \theta_d - \theta_{max}$). One interference signal with DOA@ 30° and different INRs.

In contrast, for low *INR*s (<5 dB), the effect of the interference bandwidth is unnoticeable. Additionally, the interference bandwidth has more impact on the output *SINR* as its DOA gets closer to the DOA of the desired signal. This is illustrated in **Figure 19** for the case of $\theta_{perr} = 0^o$. The effect of the interference bandwidth B_I on the depth of the nulls formed toward the interference signals is explained in **Figures 20** and **21**.

Figure 20 shows that the depth of the null formed at 30^o has a depth of –61 dB when the bandwidth of the interference signals is 0%, while it gets shallower (–48 dB) when the bandwidth of the interference signals increases (20% of the carrier frequency). This also applies to the null formed at -50^o, but with less change in the depth (as explained in **Figure 19**).

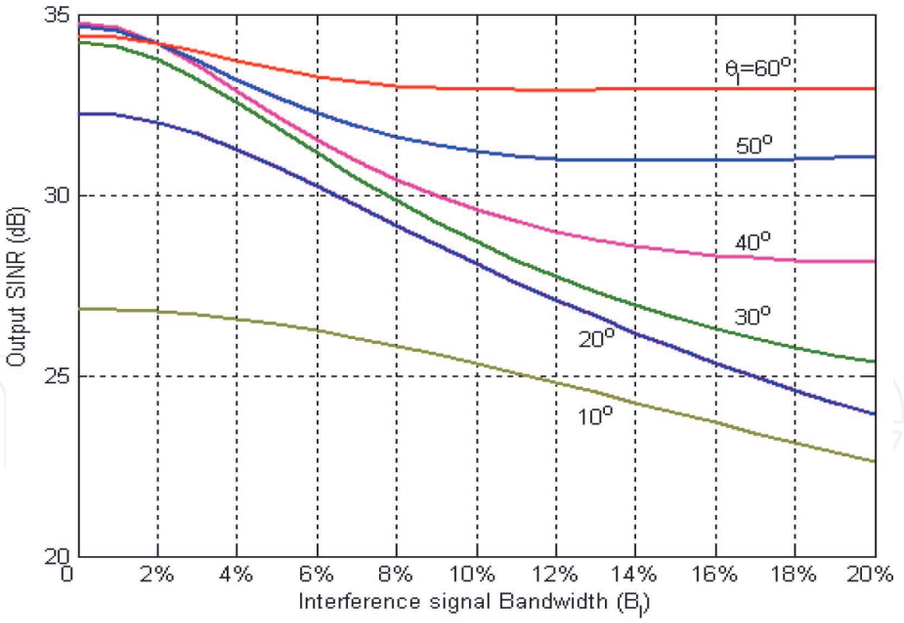

Figure 19.
Output SINR vs. interference signal bandwidth (B_I). Three-element array, $K = 0.1$, and $B_d = 0$, pointing error ($\theta_{perr} = \theta_d - \theta_{max}$). One interference signal with INR = 30 dB and different DOAs.

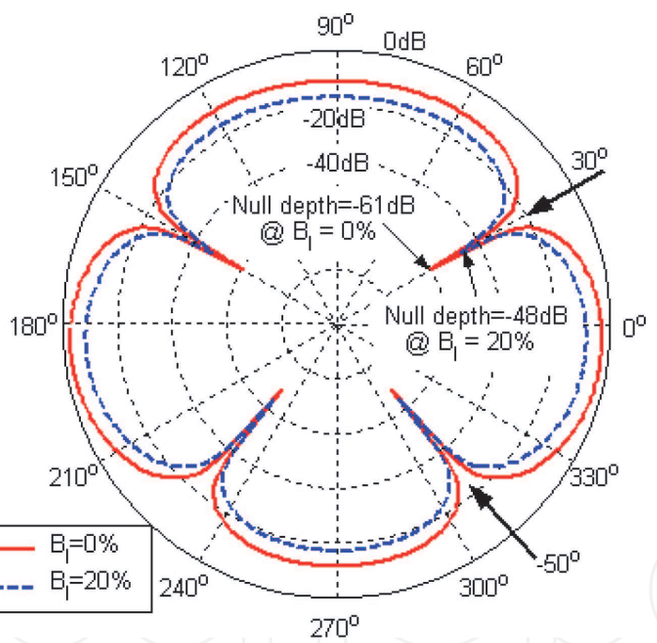

Figure 20.
Radiation patterns of a three-element array with different interference bandwidths (B_I). Input SNR = 10 dB, $B_d = 0$, $K = 0.1$, pointing error ($\theta_{perr} = \theta_d - \theta_{max}$). Two interference signals with identical bandwidths, INR's = 30 dB at 30^o and -50^o.

For more explanation, **Figure 21** illustrates the depths of the two nulls (formed at 30^o and -50^o), as a function of the interference signals bandwidth. For simplicity, we assumed here that the two bandwidths are identical. It can be seen that the nulls get shallower as the bandwidth of the interference signals increases and the close the DOA of the interference signal to the DOA of the desired signal, the more change in the null depth occurs.

As previously discussed, the N-element steered beam adaptive arrays have $N - 1$ degrees of freedom. Hence, they have the capability of efficiently nulling up to $N - 1$ interference signals. However, if more than $N - 1$ interference signals are incident on the array, the array cannot form nulls toward the interference signals. Instead, it

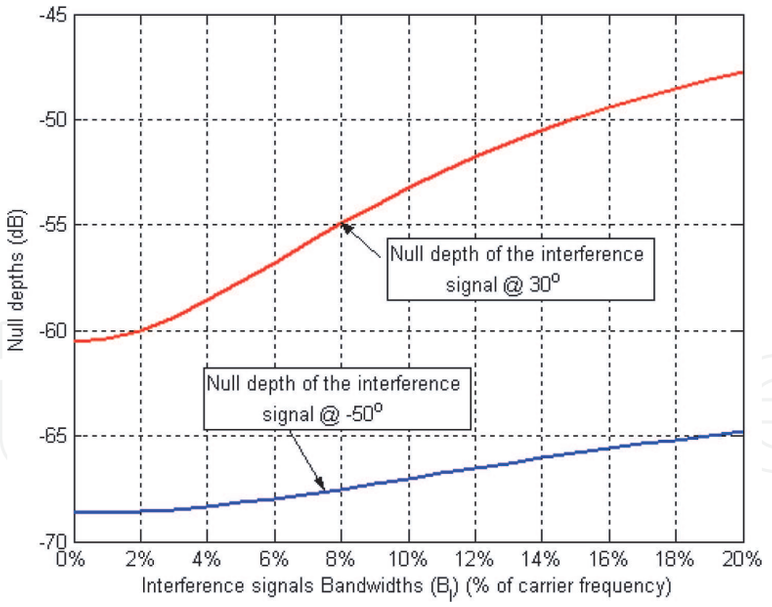

Figure 21.
Null depths formed by three-element array @ 30° and − 50° as a function of the interference bandwidth. Input SNR = 10 dB, B_d = 0, K = 0.1, pointing error ($\theta_{perr} = \theta_d - \theta_{max}$). Two interference signals with identical bandwidths, INR's = 30 dB at 30° and − 50°.

tries to form a radiation pattern such that the output *SINR* is maximized. This is shown in **Figure 22** where 6 and 12 30-dB interference signals are incident on a seven-element uniformly spaced array with uniform spacings of (λ/2).

As observed in **Figure 22**, in the case of the six interference signals with DOAs of -60^o, -50, -40^o, -45^o, $-30^o, 20^o, 30^o$, and 60^o, we can see that the array has effectively nulled these signals, while in the case of the twelve interference signals

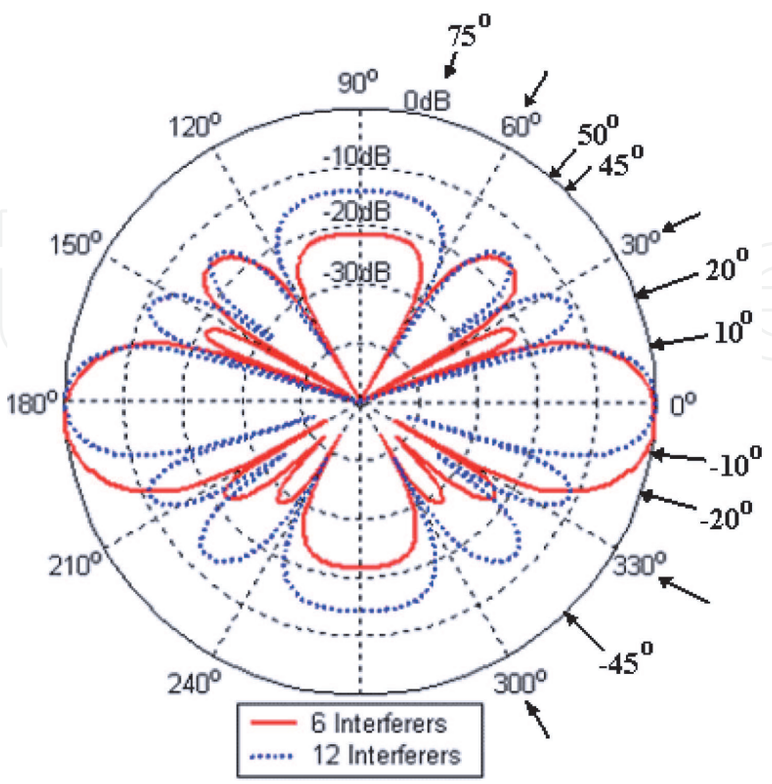

Figure 22.
Radiation patterns for the seven-element uniformly spaced adaptive array with a different number of interference signals with INR's = 30 dB. SNR = 20 dB with pointing error (θ_{perr}) = 0°.

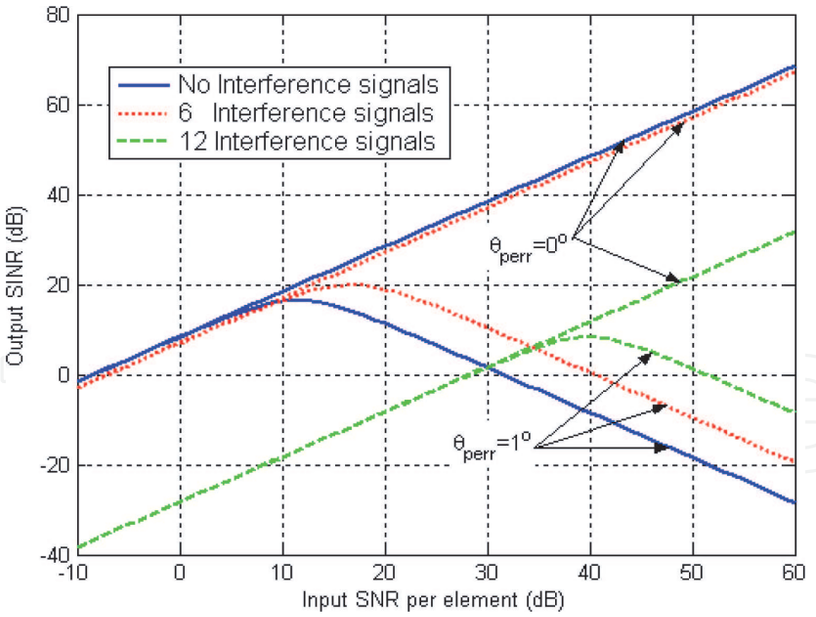

Figure 23.
Performance of the seven-element uniformly spaced adaptive array with a different number of interference signals and pointing errors. INR's = 30 dB. SNR = 20 dB.

with DOAs of -20^o, -30^o, -60^o, -45^o, $-10^o, 10^o, 20^o, 30^o, 45^o, 50^o, 60^o$, and 75^o, the array could not form nulls toward these signals, but it arranged the radiation pattern in such a way that the least amount of interference power is allowed (e.g., by forming a null between two close interference signals).

However, the presence of a large number of interference signals adds more interference power to the array output, which lowers the output *SINR*. This is illustrated in **Figure 23**, where the output *SINR* for the six effectively nulled interference signals is very close to the situation where interference signals do not exist. Clearly, both of these cases show much better performance of the adaptive array when 12 interference signals are present. Significantly, the array has more sensitivity to pointing errors in the absence of interference signals. This explains the enhancement of the output *SINR* for θ_{perr} as the input *SNR* increases.

5. Conclusions

In this chapter, we have presented and discussed the analytical formulation of the steered beam adaptive array, and we have studied the performance of the uniformly spaced steered beam adaptive array from several perspectives. It is found that by increasing the number of array elements, its directivity increases and as a result, its sensitivity to pointing errors increases as well. We also found that the greater the desired signal dynamic range (in terms of input *SNR*/element), we wish to accommodate, the less pointing error we should have. This also applies when the input *SNR*/element of the desired signal increases.

It has been found also that low values (<0.001) and high values (>0.2) of the feedback loop gain of the array have a negative effect on the performance of the array. Therefore, moderate values of feedback loop gain are preferred. It is assumed that the bandwidth of the feedback loop is large enough to accommodate the processed signals; otherwise, the adaptation process would behave erroneously.

The effect of the interference signals on the array is less if their *INR*s and bandwidths have low values. Additionally, it has been found that if the DOA of the

interference is far away from the DOA of the desired signal, its effect is less pronounced. Moreover, it is shown that if the number of the interference signals is less than the degrees of freedom of the array, the effect on the performance is less noticeable, whereas, when the number of interferers exceeds the degrees of freedom of the array, the output *SINR* is significantly affected.

Author details

Amin H. Al Ka'bi
Australian College of Kuwait, Kuwait

*Address all correspondence to: a.kabi@ack.edu.kw

References

[1] Oluwole AS, Srivastava VM. Smart antenna for wireless communication systems using spatial signal processing. Journal of Communications. 2017;**12**(6): 328-339

[2] Hum SV, Carrier J. Reconfigurable reflect-arrays and array lenses for dynamic antenna beam control: A review. IEEE Transactions on Antennas Propagation. January 2014;**62**(1):183-198

[3] Jones, Joshua A. et al. "The Poincaré-sphere approach to polarization: Formalism and new labs with Poincaré beams." American Journal of Physics, vol. 84, pp. 822-835, 2016

[4] Florencio R, Encinar JA, Toso G. Reflect-array antennas for dual polarization and broadband telecom satellite applications. IEEE Transactions on Antennas Propagation. April 2015; **63**(4):1234-1246

[5] Compton RT. On the performance of a polarization sensitive adaptive array. IEEE Transactions on Antennas Propagation. September 1981;**29**:718-725

[6] Supakwong S. Diversely Polarized Antenna Array Systems [a thesis submitted in fulfillment of requirements for the degree of Doctor of Philosophy and the Diploma of Imperial College London]. 2009

[7] K. Louertani1, R. Guinvarc, N. Ribière, and M. Hélier, "Study of the Radiated Polarization of an Antenna Array with Circular Polarization," Electromagnetics Research C, Vol. 24, pp. 173–183, DOI: 10.2528/ PIERC11061706, September 2011.

[8] Parhizgar N. A new mutual coupling compensation method for receiving antenna array-based DOA estimation. Archives of Electrical Engineering. 2018;**67**(2), pp. 419–431. DOI: 10.24425/119650

[9] Al-Ka'bi A, Bialkowski M, Homer J. Performance comparison between uniformly and non-uniformly spaced adaptive antennas with respect to tolerance to pointing errors. Journal of Microwave and Optical Technology Letters. November 2006;**48**(11): 2233-2237. DOI: 10.1002/mop.21904, EID: 2-s2.0-33749354892

[10] Lei L, Zhang G, Doviak RJ. Theoretical Analysis of Polarization Characteristics for Planar and Cylindrical Phased Array Radars. International Institute for Population Sciences (IIPS). New Orleans, LA, USA, 2012

[11] Lee KH, Cho TJ. Performance analysis of noise signal reduction using novel MUSIC method of adaptive arrays. Journal of Communications. 2017;**12**(6):347-352

[12] Balanis CA. Antenna Theory, Analysis and Design. 4th ed. New York: John Wiley & Sons Inc.; 2005. ISBN: 978-1-118-64206-1

[13] Dahri MH, Jamalueddin M. Polarization diversity and adaptive beam-steering for 5G reflect-arrays: A review. IEEE Access. April 2018;**6**: 19451-19464

[14] Ghaderi B, Parhizgar N. Resource allocation in MIMO systems specific to radio communication. Archives of Electrical Engineering. 2019;**68**(1): 91-100. DOI: 10.24425/aee.2019.125982